LETTER

https://doi.org/10.1038/s41586-019-0943-7

Photonic topological insulator in synthetic dimensions

Eran Lustig[1,4], Steffen Weimann[2,4], Yonatan Plotnik[1], Yaakov Lumer[3], Miguel A. Bandres[1], Alexander Szameit[2] & Mordechai Segev[1]*

Topological phases enable protected transport along the edges of materials, offering immunity against scattering from disorder and imperfections. These phases have been demonstrated for electronic systems, electromagnetic waves[1–5], cold atoms[6,7], acoustics[8] and even mechanics[9], and their potential applications include spintronics, quantum computing and highly efficient lasers[10–12]. Typically, the model describing topological insulators is a spatial lattice in two or three dimensions. However, topological edge states have also been observed in a lattice with one spatial dimension and one synthetic dimension (corresponding to the spin modes of an ultracold atom[13–15]), and atomic modes have been used as synthetic dimensions to demonstrate lattice models and physical phenomena that are not accessible to experiments in spatial lattices[13,16,17]. In photonics, topological lattices with synthetic dimensions have been proposed for the study of physical phenomena in high dimensions and interacting photons[18–22], but so far photonic topological insulators in synthetic dimensions have not been observed. Here we demonstrate experimentally a photonic topological insulator in synthetic dimensions. We fabricate a photonic lattice in which photons are subjected to an effective magnetic field in a space with one spatial dimension and one synthetic modal dimension. Our scheme supports topological edge states in this spatial-modal lattice, resulting in a robust topological state that extends over the bulk of a two-dimensional real-space lattice. Our system can be used to increase the dimensionality of a photonic lattice and induce long-range coupling by design, leading to lattice models that can be used to study unexplored physical phenomena.

Despite different manifestations in many physical systems, topological insulators usually rely on spatial lattices, and the wavepackets propagating in the lattice (electrons, photons or phonons) are subjected to gauge fields, giving rise to topological phenomena. However, lattices may take forms other than a spatial arrangement of sites: they can be assigned to a ladder of atomic states, photonic cavity modes or spin states[13,20,21]. Using one (or more) of these ladders in a non-spatial—synthetic—degree of freedom requires that the coupling between the synthetic sites and the resulting gauge fields is introduced as an additional external perturbation. In contrast to traditional topological insulators based on a spatial lattice, transport for topological insulators in synthetic dimensions does not occur at the spatial edges of the system, but at the edges of synthetic space. For example, the lowest and highest modes in a system can serve as synthetic edges. Using this concept, a topological edge state on a lattice with one spatial dimension and one synthetic dimension—the atomic spin state—has been demonstrated in cold atoms[14,15,23]. Other synthetic ladders, such as optical lattice clocks[24] and atomic momentum states of a Bose–Einstein condensate[25], have been used to demonstrate topological phenomena in synthetic dimensions in cold atoms. A related proposal suggested achieving synthetic dimensions by shaking harmonic traps containing cold atoms[26]. This approach uses the modes of a harmonic potential (instead of internal degrees of freedom) as the synthetic dimension, hence it allows the creation of an unlimited number of synthetic states and a high degree of control in fabricating elaborate lattices.

Creating photonic topological phenomena in synthetic dimensions has been an important research goal for some time now, because photonics offers ways to experiment with physical phenomena that are otherwise very difficult to realize in other systems (for example, nonlinearity, non-Hermiticity, exceptional points and nonlocal nonlinearities). The use of synthetic dimensions has been proposed to generate high-dimensional optical solitons[18] and was demonstrated in experiments of topological pumping[27], in which a photonic lattice was mapped onto a corresponding quantum Hall lattice with twice its spatial dimensions. Similarly, photonic topological insulators in synthetic dimensions have been proposed with the synthetic space generated through cavity modes[19–21], which offers not only an unlimited number of states but also infinite lifetime—both of which are great advantages for large-scale lattices. Thus far, however, photonic topological insulators in synthetic dimensions have not been demonstrated experimentally.

Synthetic dimensions implemented via modal space, especially in photonics, allow the introduction of arbitrary geometries and gauge fields that are not available in real-space lattices. In real-space lattices, the coupling between sites is induced by the spatial proximity of the sites to each other. This nearest-neighbour coupling severely limits the range of possible lattice geometries. By contrast, coupling between sites in synthetic space is induced externally, and applying an external perturbation corresponds to choosing the lattice coupling scheme and the gauge fields. This allows us to produce lattices with unusual features, such as long-range coupling, high dimensionality, interactions and other exotic phenomena.

Here, we design a photonic lattice that forms a topological insulator in synthetic dimensions endowed with topological edge states and directly observe the propagation of the topologically protected edge state, which resides not at the spatial edges of the system, but at the edge of synthetic space. Our scheme consists of a two-dimensional waveguide array engineered to have one synthetic dimension in modal space and one dimension in real space. This design can also be implemented in other physical systems, such as cold atoms[26] and acoustics.

We construct the photonic topological insulator in synthetic dimensions as follows. We first consider a one-dimensional array of N evanescently coupled waveguides arranged along the y axis and propagating in the z direction (Fig. 1a). This array has N propagating eigenmodes, which propagate with different propagation constants. We position the waveguides so that they form a J_x lattice with the propagation constants of its modes equally spaced[28,29]. Thus, these modes form an equally spaced ladder of modes in synthetic space. The eigenmodes of the lattice in Fig. 1a are not coupled. For example, if a wavepacket occupying the first mode is launched at the lattice input, it remains in the first mode throughout propagation, until it reaches the lattice output (purple ellipse in Fig. 1a). To support transport in the modal dimension, coupling between modes is required. To couple the modes, we spatially

[1]Physics Department and Solid State Institute, Technion–Israel Institute of Technology, Haifa, Israel. [2]Institut für Physik, Universität Rostock, Rostock, Germany. [3]Department of Electrical and Systems Engineering, University of Pennsylvania, Philadelphia, PA, USA. [4]These authors contributed equally: Eran Lustig, Steffen Weimann. *e-mail: msegev@technion.ac.il

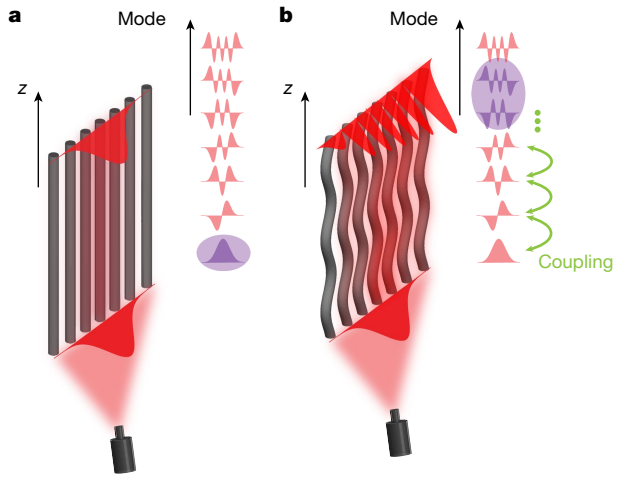

Fig. 1 | Forming a one-dimensional lattice in a synthetic modal dimension. a, One-dimensional lattice with a spectrum of $N = 7$ eigenmodes with equally spaced propagation constants. **b**, Oscillating the lattice in the longitudinal direction causes each eigenmode (of the straight lattice) to couple to its nearest neighbours, forming a lattice of coupled modes.

oscillate the one-dimensional waveguide array along its longitudinal dimension (z dimension; Fig. 1b). The period of the oscillations, Ω, is designed to induce coupling between modes that have adjacent propagation constants and creates a 'lattice of coupled modes' in the synthetic modal dimension. If a wavepacket occupying, for example, the first mode of the non-oscillating lattice is launched at the input of the oscillating lattice, it will couple to higher modes—that is, climb the modal ladder—until it constitutes a superposition of high modes at the lattice output (purple ellipse in Fig. 1b).

Next, we consider arranging M such oscillating one-dimensional arrays next to each other, at equal distances along the x axis (Fig. 2a, b). Here, the one-dimensional arrays (all oscillating in z) are columns in the y direction of a two-dimensional lattice (Fig. 2b). This system can also be viewed as a two-dimensional lattice with one of its dimensions being a synthetic dimension (Supplementary Information). The first dimension is the ordinary spatial dimension x (horizontal axis in Fig. 2a, b) whereas the second dimension is the mode spectrum of each column (vertical axis in Fig. 2a). For example, the site (3,5) in our synthetic lattice represents light occupying the third mode of the fifth real-space column in the horizontal direction x. This approach can be directly extended to demonstrate high-dimensional lattices and lattices incorporating long-range couplings (see Methods section 'Increasing the dimensionality of the lattice').

The lattice just described already contains a synthetic dimension: the modal space. However, it does not yet display topological edge states. To do that, we now add a gauge field in the synthetic dimension by introducing a phase shift in the oscillations between each pair of adjacent columns of the oscillating waveguides (Fig. 2c). The oscillations in all columns have the same frequency and amplitude but oscillations in adjacent columns differ by a constant non-zero phase. This phase difference induces an effective magnetic field for photons in the synthetic lattice, thereby opening a topological bandgap displaying topologically protected transport of edge states.

Our model is described in real space by the Hamiltonian:

$$H = -\sum_{m,n} t_{mn}(z)\, c^{\dagger}_{m+1,n} c_{m,n} - \sum_{m,n} p_n\, c^{\dagger}_{m,n+1} c_{m,n} \exp\left[i d_{y,n} k_0 \Omega R \cos(\Omega z + \phi_m)\right] + \text{H.C.} \quad (1)$$

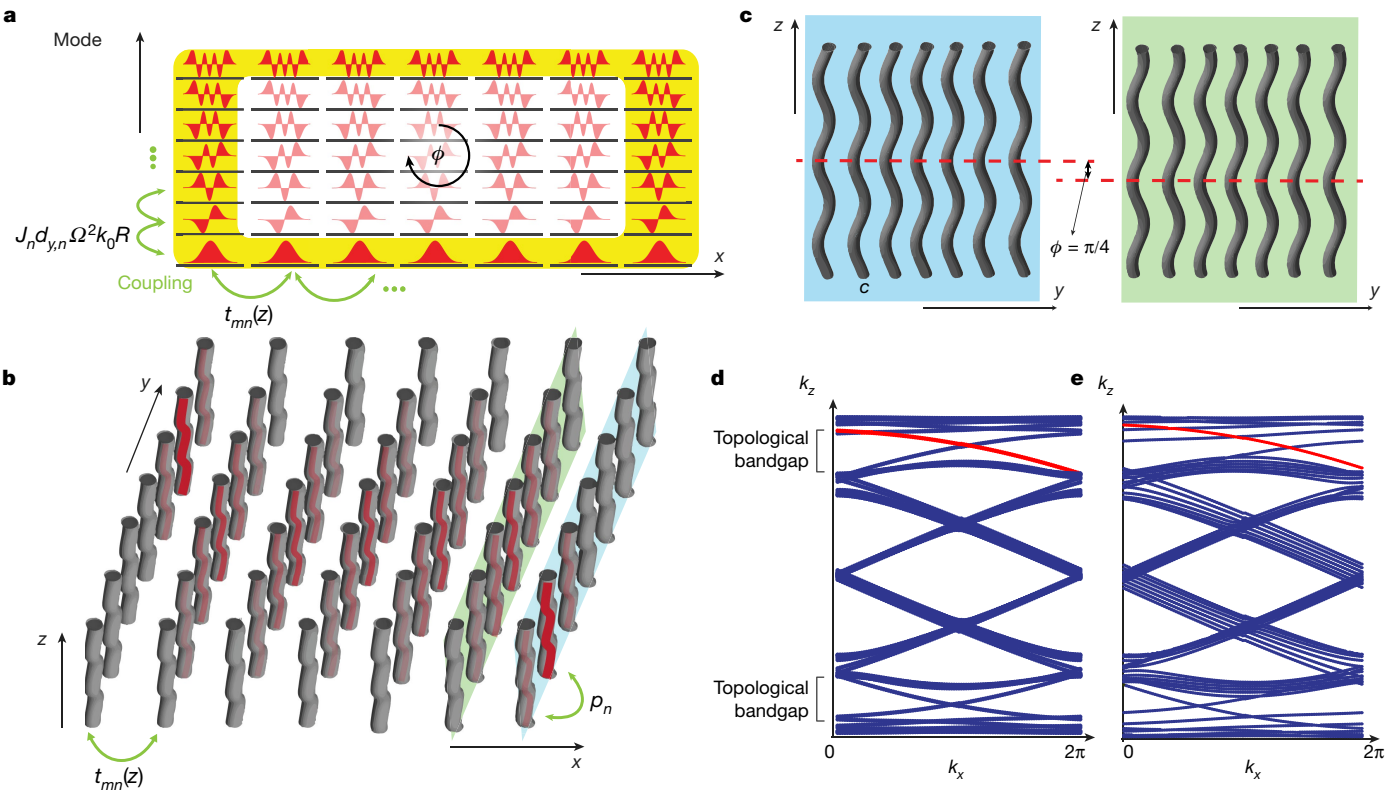

Fig. 2 | Two-dimensional synthetic-space lattice. a, **b**, Synthetic-space lattice (**a**) corresponding to a two-dimensional lattice of waveguides (**b**). The edge state of synthetic space (yellow in **a**) resides in the bulk of the waveguide array (red in **b**). $t_{mn}(z)$ and $J_n d_{y,n} \Omega^2 k_0 R$ are the coupling coefficients of the (m,n) site in synthetic space and $t_{mn}(z)$ and p_n are the couplings in real space. **c**, Phase shift between two adjacent columns of the waveguide array of **b**. **d**, Floquet band structure of a lattice with $\Omega = 70\ \text{m}^{-1}$, $R = 5\ \mu\text{m}$ and $\phi = \pi/4$, with the edge state of **a** and **b** marked in red. **e**, Floquet band structure under random disorder in the coupling between waveguides.

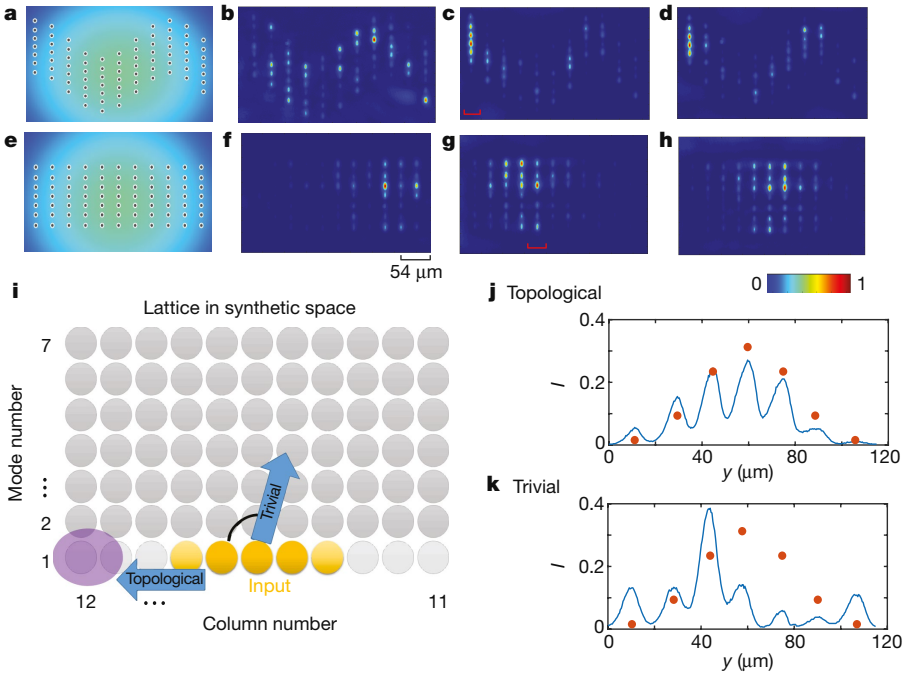

Fig. 3 | Experimentally observed evolution of a topological edge state in synthetic dimensions and in the trivial synthetic lattice. a, Illustration of a beam launched into the topological lattice ($\phi = \pi/4$, $\Omega = 87\ \mathrm{m}^{-1}$, $R = 18\ \mu\mathrm{m}$). The colour scale is for illustrating the intensity distribution on the lattice input facet. **b–d**, Experimentally obtained output beams at incidence angles without edge states ($\theta \approx 0$; **b**) and with edge states ($\theta \approx \pi/10$ in **c**; $\theta \approx \pi/5$ in **d**). Peak intensity is set to 1. **e–h**, Same as **a–d**, but for a trivial lattice. **i**, Illustrated evolution in synthetic space. The input beam (yellow) excites the lowest mode of the middle columns. In the topological lattice, the beam at the edge state evolves to the first mode of the leftmost column (purple). In the trivial lattice, the beam is in the middle of the bulk but evolves to higher modes. **j**, Normalized intensity (I) cross-section (blue line) measured at the columns indicated by the red bracket in the topological lattice of **c**. The sum of peak intensities is normalized to 1. **k**, Same as **j**, but for the trivial lattice in **g**. Orange circles in **j** and **k** indicate the calculated intensity profile of the first mode.

where $c^{\dagger}_{m,n}$ and $c_{m,n}$ are the creation and annihilation operators of the real space sites, respectively, $m = \{1,\ldots, M\}$, $n = \{1,\ldots, N\}$, p_n and $t_{mn}(z)$ are the vertical (y) and horizontal (x) coupling coefficients in real space, respectively, as depicted in Fig. 2b, R is the amplitude of the oscillations in the longitudinal z direction (which has the role of time in the corresponding Hamiltonian described by equation (1)), $k_0 = 2\pi n_0/\lambda$ is the wavenumber in the ambient medium (λ is the wavelength), $d_{y,n}$ is the distance in y between site n and site $n+1$, ϕ_m is the phase of the oscillations of the mth column and 'H.C.' stands for Hermitian conjugate. The coupling coefficients between the modes are given by $J_n d_{y,n}\Omega^2 k_0 R$, where J_n represents the unitless coupling coefficients p_n of a J_x lattice (see Supplementary Information)[28]. Unlike synthetic dimensions relying on atomic transitions, the coupling of the modes here changes only slightly between the different modes. In this two-dimensional setting all columns oscillate parallel to the y–z plane, at the same frequency Ω and amplitude R, but each column oscillates at its own phase, ϕ_m. It is the oscillation phase, ϕ_m, that makes this lattice topological, by realizing an artificial gauge field in the synthetic lattice. Mathematically, the transformation to the lattice in synthetic space is carried out by the unitary matrix U that diagonalizes the Hamiltonian $H(t_{mn} = 0, R = 0)$—that is, U diagonalizes the Hamiltonian H in equation (1) when the coupling between columns and the radius of oscillation are set to zero. We note that U converts the basis of representation to modes of separate non-oscillating columns. Using U, the Hamiltonian of the synthetic lattice, $\widetilde{H}$, is obtained by $\widetilde{H} = U^{\dagger}HU$, where H is the Hamiltonian with non-zero R and t_{mn}.

Choosing R, ϕ_m and Ω corresponds to choosing the gauge fields in the Hamiltonian $\widetilde{H}$. For our purposes, we choose $\phi_m = \phi m$, so that the oscillations have a phase shift ϕ between adjacent columns (Fig. 2c). Consequently, light accumulates the phase difference ϕ upon encircling a plaquette (the shortest closed path in the lattice) in synthetic space (Fig. 2a). Introducing a phase ϕ breaks z-reversal symmetry, and the chirality induced by ϕ is an effective magnetic field in the synthetic-space Hamiltonian $\widetilde{H}$ (see Supplementary Information). Consequently, the Hamiltonian of the synthetic lattice $\widetilde{H}$ is similar to the Hamiltonian of the Hofstadter model, and therefore the real-space lattice of H has the spectrum of a two-dimensional topological insulator. Figure 2d displays the calculated eigenmodes of the Hamiltonian (equation (1)) when periodic boundary conditions are applied in the x direction, and R, ϕ_m and Ω are chosen appropriately. The states marked in red are topological edge modes in a topological bandgap but they are not at the edge of the lattice in real space. Instead, they reside at the edge of the lattice in synthetic space (yellow frame in Fig. 2a) and in the bulk of the lattice in real space (red curves in Fig. 2b). See Methods section 'Dynamics of the wavepacket near and on the corner of synthetic space' for a description of the propagation of the topological edge state of our synthetic-space lattice.

Similarly to the edge states of a two-dimensional photonic Floquet topological insulator[4], the topological edge modes of our synthetic system are immune to disorder and reside in the gap. We verify this important feature of topological immunity in our experiment (which contains fabrication disorder) and in simulations (Methods section 'Numerical simulations of the theoretical model'). Figure 2d presents the Floquet spectrum (propagation constants versus transverse momentum) of the system without any disorder, and the topological edge states are clearly seen in the gap. For comparison, Fig. 2e shows the spectrum of the system with random disorder in the coupling between waveguides, which shifts and deforms the edge states but does not destroy them, even though the disorder here is strong—of the order of half the bandgap.

To study experimentally the evolution of the edge states in our synthetic topological insulator, we propagate a paraxial laser beam at $\lambda = 633$ nm through a two-dimensional lattice of waveguides, as shown in Fig. 2b. Our lattice of waveguides realizes the Hamiltonian of equation (1) (see Methods section 'Measuring the anticlockwise-propagating edge state').

We begin our experiments by coupling light to the edge state in the topological lattice and comparing its evolution to that in a trivial lattice. A Gaussian beam is incident on the input facet of the lattices, covering most of the sites of the columns at the centre (Fig. 3a, e). The beam is oblique in the x direction (with an angle θ that controls the transverse momentum k_x) but has a uniform phase in the y direction. This uniform phase in y makes the beam similar to the first mode in synthetic space; hence, the beam mainly excites the lowest mode of each column, which corresponds to the bottom edge of the synthetic lattice (Fig. 3i). We measure the intensity pattern at the output facet of the lattice after the beam has propagated for 15 cm. At angles θ where a topological edge state does not exist in both lattices, we observe that the beam evolves into the bulk of synthetic space (see, for example, Fig. 3b for $\theta = 0$). However, at a range of angles where a topological edge state does exist in the topological lattice, we observe that the beam propagates to the left side of the lattice (see, for example, Fig. 3c, d for $\theta \approx \pi/10$ and $\pi/5$, respectively), thus reaching the bottom left corner of synthetic

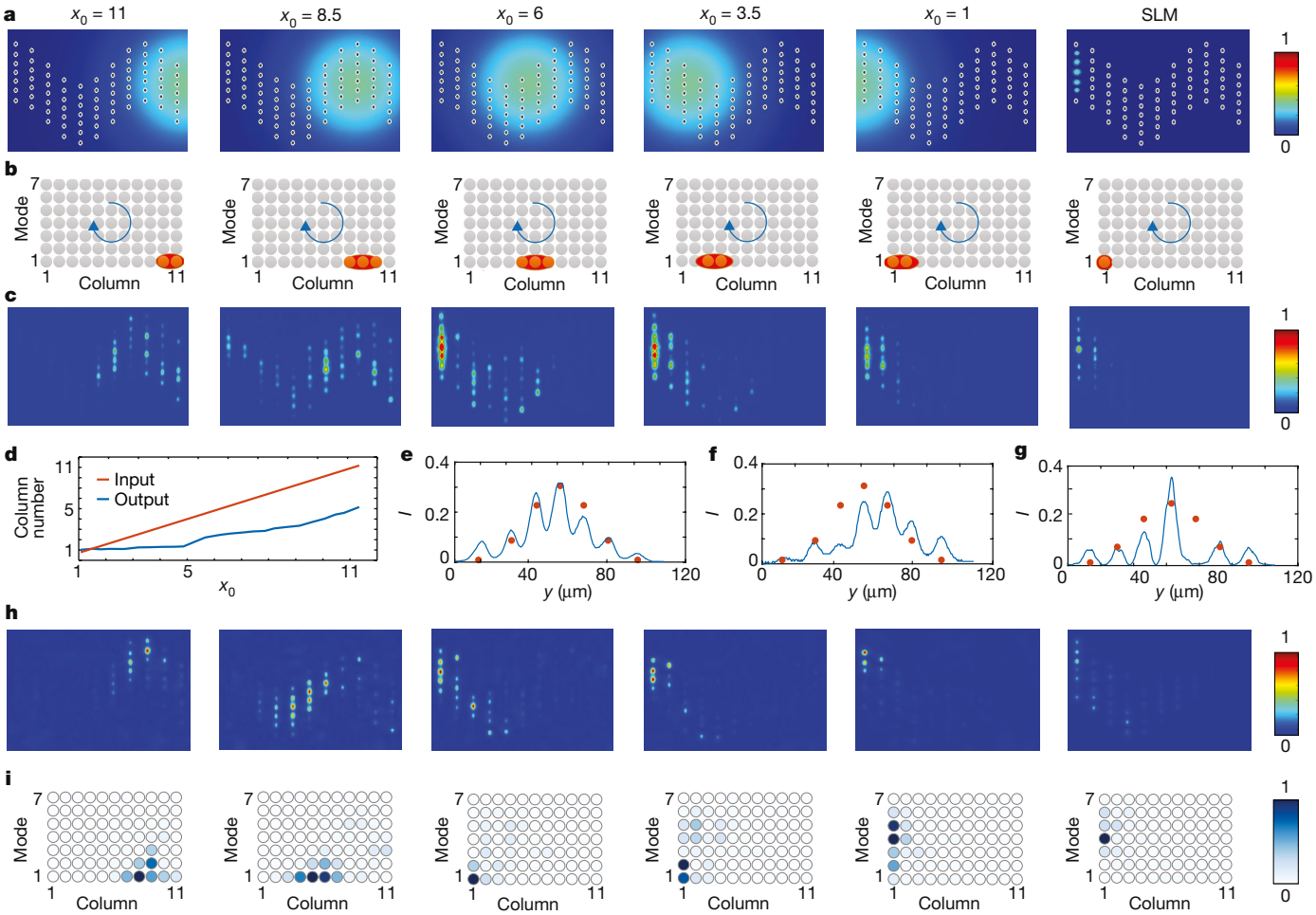

Fig. 4 | Propagation of a wavepacket along an edge state of synthetic space. The place of the images from left ($x_0 = 11$) to right ($x_0 = 1$) corresponds to different locations of the incident beam (x_0). The rightmost image corresponds to exciting only the first mode of the leftmost column using a spatial light modulator (SLM). **a**, Illustration of the intensity distribution (colour scale) of an incident narrow Gaussian beam directed towards the input facet for each x_0. **b**, The corresponding input beam (orange) in synthetic space. **c**, **h**, Experimentally imaged (**c**) and simulated (**h**) beam intensity at the output. The colour scale shows the normalized intensity; peak intensity is set to 1. **d**, Measured position of the incident Gaussian beam (orange) and mean position of the light at the output (blue). **e**–**g**, Intensity profile (blue) of the leftmost column for $x_0 = 6$ (**e**), $x_0 = 1$. The sum of peak intensities is normalized to 1. (**f**) and for the input pattern generated by the SLM (**g**), compared to the theoretical intensity profile of the first mode (orange circles). **i**, Synthetic-space description of the wavepacket propagation shown in **h**.

space (Fig. 3j). We observe the topological state within an angular range of $\Delta\theta = \pi/5$. For the same range of angles in the trivial case, the beam changes its position considerably in the x direction (Fig. 3g, h). In synthetic space, the beam propagates clockwise along the bottom edge of synthetic space until it reaches the lowest mode of the leftmost column (purple circle in Fig. 3i). This is confirmed by comparing the intensity cross-section at the leftmost column (Fig. 3j) and interference measurements (see Methods section 'Dynamics of the wavepacket near and on the corner of synthetic space') with the corresponding calculated patterns. For comparison, at the same angles (Fig. 3g, h) and in all other angles in the trivial lattice, the beam evolves into the bulk of synthetic space (blue upward-pointing arrow in Fig. 3i) since the trivial lattice has no topological edge states. Because the beam is moving up in the modal dimension of the trivial lattice, it populates high lattice modes, as proven by the intensity cross-sections (Fig. 3k).

After finding the topological edge state, we must examine whether it indeed has the two important properties of topological edge states: that it is unidirectional and that it does not scatter upon encountering an obstacle (in our case, the corner of the lattice). To show this, we launch a narrow Gaussian beam with the width of roughly three lattice sites at different regions of the lattice (Fig. 4a). We denote the centre of the Gaussian beam with x_0, where $x_0 = 11$ means that the beam is at the rightmost column and $x_0 = 1$ means that the beam is centred at the leftmost column. The rightmost images are for an even narrower excitation beam using a spatial light modulator. The narrow beam excites a narrower wavepacket at the synthetic-space edge (Fig. 4b). We choose the incidence angle of the Gaussian beam to match the calculated value that excites the edge states, which is also identified independently by the measurements in Fig. 3. Then, we measure the output intensity pattern while moving the position of the launched beam across the x axis, from the rightmost column ($x_0 = 11$) to the leftmost column ($x_0 = 1$). This corresponds to exciting the synthetic-space edge at different points along the propagation path of a beam evolving along the edge of synthetic space (Fig. 4b) and thus enables us to study effectively the evolution of a Gaussian wavepacket along the synthetic-space edge.

The experimentally imaged output beams for different values of x_0 are presented in Fig. 4c. Figure 4d–g provides the results of the analysis of Fig. 4c, and Fig. 4h, i displays the results of the simulation of a wavepacket propagating along the edge of synthetic space in our system. When the beam is launched on the right side of the lattice ($x_0 = 8.5, 11$; first and second images from the left in Fig. 4a) we find that the output beam is spread and resides in the bulk, to the left of the incoming beam (Fig. 4d). This corresponds to the beam propagating clockwise in synthetic space (first and second images from the left in Fig. 4i). When the beam is launched in the middle of the lattice

($x_0 = 6$; third image from the left in Fig. 4a), all the light accumulates in the leftmost column, mostly in the first mode (see Fig. 4e and phase information in Supplementary Information). When moving the launch beam farther to the left ($x_0 = 1, 3.5$; fourth, fifth and sixth images from the left in Fig. 4a), higher modes are populated at the leftmost column of the lattice output (Fig. 4f, g). In the sixth image from the left in Fig. 4a, b, a spatial light modulator is used to excite only the first mode of the leftmost column, resulting in high modes at the output of the leftmost column (sixth image from the left in Fig. 4c and Fig. 4g). This finding demonstrates the unidirectionality of the edge state: moving to the left causes the wavepacket to ascend the modal ladder, whereas moving to the right causes it to descend the ladder. As Fig. 4 shows, the beam excites an edge state that moves only in one direction; that is, as observed both in the experiment and in the simulation, the edge state never propagates in the opposite direction for the same bandgap (experimental measurements of the anticlockwise edge state of the lower bandgap are given in Methods section 'Repeating the experiments with different parameters'). At the same time, we observe that the beam does not scatter off the sharp (bottom-left) corner of synthetic space, which demonstrates topological protection (see also Methods sections 'Numerical simulations of the theoretical model' and 'Repeating the experiments with different parameters'). Altogether, these experiments prove that the propagation of the edge mode in our synthetic-space lattice possesses all the properties expected from topological edge modes, which in our lattice occur in synthetic space. We have therefore demonstrated a photonic topological insulator in synthetic space.

To conclude, we studied theoretically and experimentally a two-dimensional lattice that has one modal dimension and one spatial dimension and is subjected to a gauge field in synthetic space, creating a photonic topological insulator in synthetic space. Although we focused on topological phenomena, our scheme for creating synthetic lattices is modular and leads to new experimentally realizable systems. This opens the door for experiments combining high-dimensional physics and long-range couplings (see Methods section 'Increasing the dimensionality of the lattice') with a plethora of physical phenomena, including parity–time symmetry[30,31], exceptional points[32], Anderson localization and solitons. Our study paves the way to the observation of these exciting phenomena, which are currently extremely difficult to observe in other physical systems. Also, the topological edge state in our system is in the bulk in real space, which allows topological transport that is not restricted to the spatial edges of the system, but extends over the entire system. This can be important for applications such as one-way fibres[33] and topological insulator lasers in synthetic dimensions[11,12].

Online content

Any methods, additional references, Nature Research reporting summaries, source data, statements of data availability and associated accession codes are available at https://doi.org/10.1038/s41586-019-0943-7.

Received: 5 July 2018; Accepted: 13 December 2018;
Published online 18 February 2019.

1. Haldane, F. D. M. & Raghu, S. Possible realization of directional optical waveguides in photonic crystals with broken time-reversal symmetry. *Phys. Rev. Lett.* **100**, 013904 (2008).
2. Wang, Z., Chong, Y., Joannopoulos, J. D. & Soljačić, M. Observation of unidirectional backscattering-immune topological electromagnetic states. *Nature* **461**, 772–775 (2009).
3. Malkova, N., Hromada, I., Wang, X., Bryant, G. & Chen, Z. Observation of optical Shockley-like surface states in photonic superlattices. *Opt. Lett.* **34**, 1633–1635 (2009).
4. Rechtsman, M. C. et al. Photonic Floquet topological insulators. *Nature* **496**, 196–200 (2013).
5. Hafezi, M., Mittal, S., Fan, J., Migdall, A. & Taylor, J. M. Imaging topological edge states in silicon photonics. *Nat. Photon.* **7**, 1001–1005 (2013).
6. Jotzu, G. et al. Experimental realization of the topological Haldane model with ultracold fermions. *Nature* **515**, 237 (2014).
7. Aidelsburger, M. et al. Measuring the Chern number of Hofstadter bands with ultracold bosonic atoms. *Nat. Phys.* **11**, 162–166 (2015).
8. He, C. et al. Acoustic topological insulator and robust one-way sound transport. *Nat. Phys.* **12**, 1124–1129 (2016).
9. Süsstrunk, R. & Huber, S. D. Observation of phononic helical edge states in a mechanical topological insulator. *Science* **349**, 47–50 (2015).
10. Bahari, B. et al. Nonreciprocal lasing in topological cavities of arbitrary geometries. *Science* **358**, 636–640 (2017).
11. Harari, G. et al. Topological insulator laser: theory. *Science* **359**, eaar4003 (2018).
12. Bandres, M. A. et al. Topological insulator laser: experiments. *Science* **359**, eaar4005 (2018).
13. Celi, A. et al. Synthetic gauge fields in synthetic dimensions. *Phys. Rev. Lett.* **112**, 043001 (2014).
14. Mancini, M. et al. Observation of chiral edge states with neutral fermions in synthetic Hall ribbons. *Science* **349**, 1510–1513 (2015).
15. Stuhl, B. K., Lu, H.-I., Aycock, L. M., Genkina, D. & Spielman, I. B. Visualizing edge states with an atomic Bose gas in the quantum Hall regime. *Science* **349**, 1514–1518 (2015).
16. Boada, O., Celi, A., Latorre, J. I. & Lewenstein, M. Quantum simulation of an extra dimension. *Phys. Rev. Lett.* **108**, 133001 (2012).
17. Price, H. M., Zilberberg, O., Ozawa, T., Carusotto, I. & Goldman, N. Four-dimensional quantum Hall effect with ultracold atoms. *Phys. Rev. Lett.* **115**, 195303 (2015).
18. Jukić, D. & Buljan, H. Four-dimensional photonic lattices and discrete tesseract solitons. *Phys. Rev. A* **87**, 013814 (2013).
19. Luo, X.-W. et al. Quantum simulation of 2D topological physics in a 1D array of optical cavities. *Nat. Commun.* **6**, 7704 (2015).
20. Yuan, L., Shi, Y. & Fan, S. Photonic gauge potential in a system with a synthetic frequency dimension. *Opt. Lett.* **41**, 741–744 (2016).
21. Ozawa, T., Price, H. M., Goldman, N., Zilberberg, O. & Carusotto, I. Synthetic dimensions in integrated photonics: from optical isolation to four-dimensional quantum Hall physics. *Phys. Rev. A* **93**, 043827 (2016).
22. Yuan, L., Lin, Q., Xiao, M. & Fan, S. Synthetic dimension in photonics. *Optica* **5**, 1396–1405 (2018).
23. Genkina, D. et al. Imaging topology of Hofstadter ribbons. Preprint at https://arxiv.org/abs/1804.06345 (2018).
24. Kolkowitz, S. et al. Spin–orbit-coupled fermions in an optical lattice clock. *Nature* **542**, 66–70 (2017).
25. An, F. A., Meier, E. J. & Gadway, B. Direct observation of chiral currents and magnetic reflection in atomic flux lattices. *Sci. Adv.* **3**, e1602685 (2017).
26. Price, H. M., Ozawa, T. & Goldman, N. Synthetic dimensions for cold atoms from shaking a harmonic trap. *Phys. Rev. A* **95**, 023607 (2017).
27. Zilberberg, O. et al. Photonic topological boundary pumping as a probe of 4D quantum Hall physics. *Nature* **553**, 59–62 (2018).
28. Weimann, S. et al. Implementation of quantum and classical discrete fractional Fourier transforms. *Nat. Commun.* **7**, 11027 (2016).
29. Perez-Leija, A., Keil, R., Kay, A., Moya-Cessa, H., Nolte, S., Kwek, L.-C., Rodríguez-Lara, B. M., Szameit, A. & Christodoulides, D. N. Coherent quantum transport in photonic lattices. *Phys. Rev. A* **87**, 012309 (2013).
30. Makris, K. G., El-Ganainy, R., Christodoulides, D. N. & Musslimani, Z. H. Beam dynamics in PT symmetric optical lattices. *Phys. Rev. Lett.* **100**, 103904 (2008).
31. Rüter, C. E. et al. Observation of parity–time symmetry in optics. *Nat. Phys.* **6**, 192 (2010).
32. Klaiman, S., Günther, U. & Moiseyev, N. Visualization of branch points in PT-symmetric waveguides. *Phys. Rev. Lett.* **101**, 080402 (2008).
33. Lu, L., Gao, H. & Wang, Z. Topological one-way fiber of second Chern number. *Nat. Commun.* **9**, 5384 (2018).

Acknowledgements This work was supported by the German–Israeli DIP Program, by an Advanced Grant from the European Research Council and by the Israel Science Foundation. E.L. is grateful for the support of the Israel Academy of Sciences through an Adams Fellowship.

Reviewer information *Nature* thanks Ling Lu and the other anonymous reviewer(s) for their contribution to the peer review of this work.

Author contributions All authors contributed significantly to this work.

Competing interests The authors declare no competing interests.

Additional information
Extended data is available for this paper at https://doi.org/10.1038/s41586-019-0943-7.
Supplementary information is available for this paper at https://doi.org/10.1038/s41586-019-0943-7.
Reprints and permissions information is available at http://www.nature.com/reprints.
Correspondence and requests for materials should be addressed to M.S.
Publisher's note: Springer Nature remains neutral with regard to jurisdictional claims in published maps and institutional affiliations.

METHODS

Increasing the dimensionality of the lattice. Lattices in synthetic dimensions can be engineered by exploiting either internal degrees of freedom, such as the electron spin states[13–15,24,34], or by using non-internal degrees of freedom, such as the waveguide modes described here, cavity modes or any other modes created by geometrical engineering the system[20,21,26,35]. In both cases (internal and non-internal) the lattice has the ability to represent physics in dimensions higher than those of the system and to have long-range couplings in a controlled manner. These abilities enable lattices in synthetic dimensions to exhibit numerous effects that are not observed in regular spatial lattices[22,36–38]. The main advantages in using non-internal modes in photonics is the ability to scale up the system, owing to the unlimited number of available states in the synthetic dimension, and to observe its dynamics over a long time because of the absence of spontaneous decay or decoherence, as well as the ability to engineer the modes of synthetic space and their couplings to a high degree. The ability to study experimentally photonic systems in synthetic dimensions opens the door for experiments combining high-dimensional physics and a plethora of physical phenomena, ranging from parity–time symmetry[30,31,39], including in dimensions higher than one[40–42], exceptional points[31,32,43], and unidirectional invisibility[44] in high dimensions, to Anderson localization[45] under nonlocal or high-dimensional settings, high-dimensional solitons[18], topological insulator lasers[10–12] and exciton-polariton topological insulator[46], all in systems incorporating synthetic dimensions.

In this section, we elaborate on how to increase the dimensionality of the two-dimensional lattice of waveguides to more than two dimensions. There are two main avenues to do that. The first is by arranging one-dimensional oscillating columns as the unit cells of a two-dimensional lattice (Extended Data Fig. 1a). In this case, there are three dimensions: two dimensions describe the positions of the one-dimensional columns in the plane and the third dimension is the mode in each one-dimensional column (Extended Data Fig. 1b). In Extended Data Fig. 1a, each column of waveguides couples to four neighbouring columns by moving along z on the path marked by the black lines, tracing the figure '8'. The red columns move in the opposite direction with respect to the blue columns (as indicated by the direction of the black triangles in Extended Data Fig. 1a). The Floquet Hamiltonian of this motion maps to a two-dimensional triangular lattice in space[47] and the added third dimension is the modal dimension of each column, as discussed in the main text.

The second method is to design the waveguides to oscillate in z at several frequencies instead of one. For example, if the one-dimensional rows oscillate at frequency Ω, then the index of refraction n can also oscillate in z at $r\Omega$, where r is an integer (Extended Data Fig. 1c). More specifically, the refractive index can be made to vary according to $n(z) = n_0 + \gamma\cos\left(r\Omega z + \frac{\pi}{M-1}m\right)$, where γ is a unitless amplitude, n_0 is the ambient index of refraction, m is the site number in the x dimension and M is the total number of sites in an oscillating row. Oscillation at frequency $r\Omega$ couples the modes of rows spaced by $r-1$ modes. This long-range coupling appears in many lattice models and can be used to experimentally demonstrate high-dimensional physics; however, it is difficult to fabricate lattices with long-range couplings in regular spatial lattices. Considering also oscillations of the rows in space (x axis in Extended Data Fig. 1c) with frequency Ω and amplitude β results in a lattice with both short-range and long-range couplings. In this case, the first dimension is the real-space position of the row in y and two more dimensions can be encoded in the modes of the rows because multifrequency oscillations can correspond to several dimensions[48,49], forming a three-dimensional (3D) lattice. This 3D lattice can also be subjected to non-trivial effective 3D gauge fields for light by altering the relative phases of the different oscillations (Extended Data Fig. 1d). In such cases, there is no limit to the number of dimensions that can be added.

Dynamics of the wavepacket near and on the corner of synthetic space. In the main text we describe the propagation of a wavepacket along the edge of synthetic space. Here, we elaborate on this propagation and provide further analysis and results on the experimentally measured dynamics of the wavepacket near and on the corner of synthetic space.

As explained in the main text, the edges of synthetic space are not the edges of real space. The bottom edge of synthetic space, for example, means occupying the lowest mode of each column, which extends over the entire column in real space (see Fig. 2a). Thus, a wavepacket occupying the bottom edge of synthetic space will actually extend over the entire bulk of the lattice in real space, with the same phase at all lattice sites within each column. In the same vein, a wavepacket occupying the upper edge of synthetic space also extends over the entire lattice, but with π phase difference between adjacent sites within each column. The left and right edges have a completely different nature from the bottom and upper edges. Here, occupying the left edge in synthetic space also means occupying the left edge in real space because x is the spatial dimension of our lattice, and likewise for the right edge of our lattice. A wavepacket encircling the edges of the synthetic lattice will, for example, start its journey at the bottom edge of synthetic space (the lowest mode of each column), then propagate along the lower edge of synthetic space (which covers the entire bulk in real space) to the leftmost column, where it will stay and climb up the modal ladder, starting from the first mode. After reaching the highest mode, the wavepacket will start propagating rightwards over the entire bulk of real space, but occupying the high lattice modes, until it reaches the right edge. After that, the wavepacket will descend the modal ladder until it reaches the lowest mode, completing a full cycle around the edges of our synthetic lattice.

Next, we explain the properties dictated by the topology of our specific synthetic lattice. In our system, for $\phi = \pi/4$ there are two counter-propagating edge states in synthetic dimensions: one in the lowest bandgap and one in the upper bandgap (Fig. 2d, e). We focus on the state in the upper bandgap because it has a lower spatial frequency and thus it is easier to excite with a Gaussian beam (the experimental observation of the edge state of the lower bandgap is described in 'Measuring the anticlockwise-propagating edge state'). The edge state that we measure resides in some range of k_x values, which may vary in location and size owing to some inherent disorder in the fabrication of the lattice (compare, for example, the edge state in Fig. 2d with that in Fig. 2e). Because ϕ is positive, this edge state should propagate clockwise in synthetic space. Furthermore, in the upper bandgap there should be no edge states propagating anticlockwise in synthetic space. Thus, a wavepacket exciting this synthetic-space edge state should not scatter while passing the corner of synthetic space; rather, it should propagate along the leftmost column of the lattice in synthetic space. For comparison, we expect that the same wavepacket launched into the topologically trivial system (with $\phi = 0$) will strongly scatter into the bulk of synthetic space.

In our experiment, we specifically study propagation in the vicinity of the corner in synthetic space because it is the most complicated part of the dynamics. We now provide further results and conclusions related to the propagating wavepacket of Fig. 4. The propagation of the wavepacket along the edge of synthetic space, as described in the main text, starts at the lower edge of synthetic space (Extended Data Fig. 2a, b) and continues clockwise until it reaches the first mode of the leftmost column, which is the bottom-left corner of synthetic space. At this point of the propagation, we expect that the leftmost column will be occupied mostly by the first mode. To see this, we measure the intensity distribution of the light exiting the lattice in the leftmost column. We compare the measured intensity (Extended Data Fig. 2c) with the calculated intensity of the first mode (orange circles in Extended Data Fig. 2e). To confirm that this is indeed mostly the first mode, we measure the phase by interfering the light emerging from the leftmost column with the incoming Gaussian beam (Extended Data Fig. 2d). Because the peaks align on the equal-phase circle of the Gaussian beam (dashed line in Extended Data Fig. 2d), we conclude that all the light leaves the waveguides with the same phase—which matches the phase pattern of the first mode. The slight deviation from the first mode can be attributed to a small occupancy in the second mode, which is expected because the edge state occupies also the second mode as it decays into the bulk of synthetic space.

After the wavepacket reaches the corner, we expect it to continue its propagation by staying in the leftmost column (instead of coupling to other columns, as in the trivial case) and start occupying higher modes in the leftmost column. In Extended Data Fig. 3 we show the measured output light for the case in which the initial Gaussian beam is launched on the left side of the lattice, which represents a later stage in the propagation of the wavepacket (Extended Data Fig. 3a, b).

We measure the intensity (Extended Data Fig. 3c, f) and the phase (Extended Data Fig. 3d, e) of the light occupying the leftmost column in the same way as in Extended Data Fig. 2c, e. We observe that the intensity does not match the first mode (Extended Data Fig. 3f) and that the intensity peaks in Extended Data Fig. 3e do not lie perfectly on the equal-phase line (dashed line). Instead, we notice a phase difference of up to about $2\pi/3$ between adjacent sites, which means that the light does not match the first mode in its phase either. By estimating the mode occupancy of Extended Data Fig. 3c–f according to the phase and amplitude, we find that more than 50% of the light intensity is in higher modes.

Numerical simulations of the theoretical model. In the main text, we present a new scheme for achieving a topological insulator in synthetic dimensions using a two-dimensional oscillating lattice. Here we give further details on this scheme. As mentioned in the main text, we can describe our model with the tight-binding approach. The tight-binding equation for our scheme is equation (1). In Supplementary Information, we explain why equation (1) describes our lattice of waveguides and how it relates to topological insulators in synthetic dimensions. Here, we give further details on this model by studying it numerically.

Before we start, we first describe how to choose the parameters of equation (1) to fit the desired model in synthetic dimensions. Equation (1) can represent many models in synthetic dimensions for different choices of R, Ω, p_n and ϕ_m.

Choosing the couplings, p_n, and the frequency, Ω. The frequency should correspond to the spacing between the different modes in the propagation constant k_z of each column (which has the role of energy in the analogous energy Hamiltonian). If the couplings are chosen according to a J_x lattice, then the modes are equally spaced in k_z, and Ω is chosen according to that spacing.

Choosing the amplitude of oscillations, R. The amplitude of the oscillations corresponds to the strength of the coupling between the modes in synthetic space. Here, we choose R to be large enough to have substantial evolution dynamics within the finite propagation distance of our experiments and small enough so that it does not induce high-order effects that obstruct the dynamics.

Choosing the phase, ϕ_m. ϕ_m is the phase per plaquette in synthetic space. We start by determining the Floquet eigenvalues and eigenvectors of equation (1) for a finite 20×20 lattice with $\phi = \pi/2$ (the spectrum in Fig. 2d, e is for a lattice of the same size as the experimental lattice, but with seven sites in the y dimension and infinite periodicity in the x dimension, and has a periodic boundary condition of $\phi = \pi/4$). We calculate the eigenvalues (Extended Data Fig. 4a) and the distribution of one eigenvector in the gap in real space (Extended Data Fig. 4b) and synthetic space (Extended Data Fig. 4c). The spectrum clearly shows the existence of edge states, which reside in the bulk of the real-space lattice, but at the edge of synthetic space.

Finally, in Supplementary Information we show that the bulk propagation in synthetic dimensions is mathematically equivalent to the Hofstadter model under certain approximations. Consequently, it shares the same properties of the Hofstadter model, but in synthetic dimensions. However, when disorder is introduced into synthetic space, it acts differently than in real space. In real space, the disorder usually affects only the on-site energy and nearest-neighbour coupling, which are the diagonal and off-diagonal terms in a Hamiltonian of a one-dimensional lattice in the tight-binding approach (Extended Data Fig. 5a). Because the transformation to synthetic space is nonlocal, in synthetic space this disorder can have long-range coupling (Extended Data Fig. 5b). To see how the disorder in synthetic space affects our model, we calculate the Bott index[50] of the Hofstadter model with ordinary disorder (on-site and nearest-neighbours couplings) and with disorder introduced into synthetic space (Extended Data Fig. 5c). This calculation gives roughly the same result for both cases, meaning that the topology is robust.

Next, we discuss the impact of disorder that is confined in space (for example, removing a single site or several sites; Extended Data Fig. 5d). We find that the topology is not as robust as for the regular topological insulator and for the topological insulator in synthetic dimensions. Because the unitary transformation between real space and synthetic space (equation (11) in Supplementary Information) is nonlocal, disorder that is confined in real space becomes non-confined in synthetic space (Extended Data Fig. 5e) and vice versa. Thus, although strongly confined defects may affect the robustness of the topological edge state in synthetic dimensions, the state is nevertheless robust to a range of defects that are not confined spatially in real space, but are confined in synthetic space.

Measuring the anticlockwise-propagating edge state. In our experiment we focused on measuring the edge state that propagates clockwise in synthetic space. The Hofstadter model includes also an edge state that propagates in the reverse direction—anticlockwise—in a different bandgap. In our experimental system and its simulations, this second edge state is more difficult to measure and to excite. However, we can excite it by using a spatial light modulator (SLM). We excite the first mode in the rightmost column with the SLM, which corresponds to exciting the bottom-right corner in synthetic space. As a result, part of the light couples to the clockwise edge state (and propagates to the bulk) and part to the anticlockwise state (and propagates on the rightmost column, increasing in modes). The light that couples to the anticlockwise edge state is concentrated on a smaller number of sites than the light that couples to the bulk. This fact results in a clear measurement of the anticlockwise edge state in the output intensity image. Extended Data Fig. 6 shows experimental results demonstrating the anticlockwise edge state.

Extended Data Fig. 6a, d shows the excitation in real space (first mode of the rightmost column) of the topological and trivial lattices, respectively. The measured output shows that for the topological case (Extended Data Fig. 6b) light propagates along the edge of synthetic space, rising in modes in the rightmost column (the mode at the output is clearly not the first mode, because the third waveguide from the bottom has zero light occupancy). By contrast, in the trivial case (Extended Data Fig. 6e) light propagates to the bulk and increases in mode, thus propagating diagonally in the space–mode lattice (Extended Data Fig. 6f).

Repeating the experiments with different parameters. To further establish that the dynamics that we observe in our experimental system is indeed of topological nature and robust in the presence of disorder, we fabricate a second lattice, with different parameters than the sample used to obtain the data presented in the main text, but with the same topological features. We repeat the experiments and measure the synthetic-space edge state in this new sample. Extended Data Fig. 7a, b presents the incident light beam in real space and in synthetic space, whereas Extended Data Fig. 7c, d shows the corresponding experimental data and simulation results at the output facet of the photonic lattice. We observe clear localization at the leftmost edge, which begins at low modes and climbs the modal ladder to higher modes with the initial beam moving to the left. Extended Data Fig.7e shows the corresponding image in synthetic space.

Designing the experimental lattice in synthetic dimensions. Here, we provide further technical details on the waveguide lattices described the main text, in terms of their relation to the tight-binding model and their fabrication. We fabricated lattices with $\phi = \pi/4$ (topological) and with $\phi = 0$ (topologically trivial). The lattices consist of 7×11 waveguides fabricated in fused silica using the direct laser writing technique[51]. The oscillation parameters (Ω, R) and the spacing between waveguides (in x) are such that the coupling coefficient in the x dimension and in the synthetic dimension are close to one another and are sizeable enough to obtain considerable evolution during propagation in our lattice. The light propagates according to the paraxial equation:

$$i\frac{\partial}{\partial z}\psi = -\frac{1}{2k_0}\nabla^2\psi(x,y,z) + \frac{k_0\Delta n(x,y,z)}{n_0}\psi(x,y,z) \qquad (2)$$

In equation (2) $\psi(x, y, z)$ is the electric-field envelope function, defined by $\boldsymbol{E}(x, y, z) = \psi(x, y, z)\exp(ik_0z - i\omega t)$, where $\boldsymbol{E}(x, y, z)$ is the electric field, z is the propagation axis, the Laplacian ∇^2 is restricted to the transverse $(x - y)$ plane, $\omega = 2\pi c/\lambda$ is the optical frequency and c is the velocity of light. Here, $-\Delta n(x, y, z)$ is the 'effective potential', that is, the variation in the refractive index relative to the ambient refractive index of the medium, n_0. We launch a Gaussian beam into the lattice, excite the edge state in synthetic space at $z = 0$ and measure the intensity at the output face of the lattice using a charge-coupled device camera.

We now describe the process of designing the experimental photonic lattice that we used. The process included several steps: first, we fabricated a single elliptical waveguide and measured the intensity distribution of the propagating modes in both its major and minor axes (orange line in Extended Data Fig. 8a, b). This process was carried out shortly before the fabrication of the lattice to avoid inaccuracies due to some drift in the experimental system, which occurs naturally over time. Following this, we measured the coupling of two fabricated waveguides as a function of the distance between them and obtained exponential curves (Extended Data Fig. 8c, d).

On the basis of the measurements presented in Extended Data Fig. 8a–d, we deduced the spatial distribution of the index of refraction of a single site, Δn_{site}. We compared the modes of the simulated waveguides with the experimental waveguides (blue points in Extended Data Fig. 8a, b), and using Δn_{site} we simulated a single J_x lattice. The eigenvalues of the lattice are shown in Extended Data Fig. 8e. The first five eigenvalues are perfectly aligned, as required, but modes 6 and 7 tilt upwards from the straight blue line. The reason for this deviation is the relatively close proximity of the waveguides in the experiment, which slightly violates the tight-binding approximation and therefore reduces the efficiency of the coupling of modes 6 and 7 in the experiment. Reducing the efficiency of the coupling in the two highest modes was a compromise made because of the short propagation length in the experiment— separating the waveguides from each other further reduced the average coupling and slowed down the overall dynamics in z. Next, we used the beam propagation method to verify that the eigenmodes of a single oscillating J_x lattice were all coupled to one another and verified the existence of the topological edge state in synthetic dimensions in the exact lattice that we fabricated (these are the simulations shown in Fig. 4c). Finally, after simulating the system using data extracted from the experimental system, we fabricated the lattice and performed the experiments described in the main text. Our waveguide structure had 7×11 waveguides, a radius of $R = 18$ μm and $\Omega = 0.87$ rad cm^{-1}; the distances of the J_x lattice were (17.49, 15.67, 15.15, 15.15, 15.67, 17.49) μm, the spacing in the x axis was 27 μm, the phase difference between the oscillating waveguides was $\pi/4$ and our probe wavelength was $\lambda = 633$ nm. The coupling curves were $C_x = 2,670.08e^{-\frac{x}{5.7772\times10^{-6}}}$ and $C_y = 2,118.41e^{-\frac{y}{5.90928\times10^{-6}}}$ in units of m^{-1} and the ambient refractive index was $n_0 = 1.45$. The value of $d_y k_0 R\Omega$ is theoretically about 0.3, where $d_y = \max(d_{y,n})$. The fast-rotating-wave approximation requires $d_y k_0 R\Omega \ll 1$. However, according to our simulations 0.3 is small enough to preserve edge states in a gap. The simulation for the band structure shown in Fig. 1 was done with the following parameters: $R = 5$ μm, $\Omega = 69.1448$ m^{-1}, coupling in y of $C_y = 10.943$ m^{-1} and $k_0 = 1.919 \times 10^7$ m^{-1}. We fabricated the waveguides in 15-cm-long samples of fused silica glass (Corning 7980) using the femtosecond laser writing method. We used pulses created by a Coherent RegA optical parametric amplifier seeded with pulses from a Ti:sapphire Mira 900 laser carrying energy of 450 nJ per pulse, at 800 nm and 100 kHz repetition rate. An Aerotech ALS 130 positioning system together with a microscope objective (numerical aperture, 0.35) provided highly accurate focusing of the laser beam ranging between 50 μm and 800 μm under the sample surface. The laser pulses modified the refractive index of the sample (by up to 7×10^{-4}) at the focal point and scanned point by point by moving the sample with a speed of 100 mm min^{-1}. This created waveguides with a mode field with principal axes of 10.4 μm and 8 μm at 632.8 nm wavelength. Propagation losses and birefringence were estimated at 0.2 dB cm^{-1} and 10^{-7}, respectively. For more details on the fabrication, see ref. [51].

Data availability

The data that support the findings of this study are available from the corresponding author upon reasonable request.

34. Livi, L. F. et al. Synthetic dimensions and spin–orbit coupling with an optical clock transition. *Phys. Rev. Lett.* **117**, 220401 (2016).
35. Fang, K. et al. Generalized non-reciprocity in an optomechanical circuit via synthetic magnetism and reservoir engineering. *Nat. Phys.* **13**, 465–471 (2017).
36. Price, H. M., Ozawa, T. & Carusotto, I. Quantum mechanics with a momentum-space artificial magnetic field. *Phys. Rev. Lett.* **113**, 190403 (2014).
37. Suszalski, D. & Zakrzewski, J. Different lattice geometries with a synthetic dimension. *Phys. Rev. A* **94**, 033602 (2016).
38. Goldman, N., Budich, J. C. & Zoller, P. Topological quantum matter with ultracold gases in optical lattices. *Nat. Phys.* **12**, 639–645 (2016).
39. Bell, B. A. et al. Spectral photonic lattices with complex long-range coupling. *Optica* **4**, 1433–1436 (2017).
40. Ge, L. & Stone, A. D. Parity–time symmetry breaking beyond one dimension: the role of degeneracy. *Phys. Rev. X* **4**, 031011 (2014).
41. Bender, C. M., Hassanpour, N., Klevansky, S. P. & Sarkar, S. PT-symmetric quantum field theory in D dimensions. *Phys. Rev. D* **98**, 125003 (2018).
42. Kremer, M., Biesenthal, T., Heinrich, M., Thomale, R. & Szameit, A. Demonstration of a two-dimensional PT-symmetric crystal: bulk dynamics, topology, and edge states. Preprint at http://arxiv.org/abs/1809.00041 (2018).
43. Hodaei, H. et al. Enhanced sensitivity at higher-order exceptional points. *Nature* **548**, 187–191 (2017).
44. Lin, Z. et al. Unidirectional invisibility induced by PT-symmetric periodic structures. *Phys. Rev. Lett.* **106**, 213901 (2011).
45. Schwartz, T., Bartal, G., Fishman, S. & Segev, M. Transport and Anderson localization in disordered two-dimensional photonic lattices. *Nature* **446**, 52–55 (2007).
46. Klembt, S. et al. Exciton-polariton topological insulator. *Nature* **562**, 552–556 (2018).
47. Noh, J. et al. Experimental observation of optical Weyl points and Fermi arc-like surface states. *Nat. Phys.* **13**, 611–617 (2017).
48. Martin, I., Refael, G. & Halperin, B. Topological frequency conversion in strongly driven quantum systems. *Phys. Rev. X* **7**, 041008 (2017).
49. Yuan, L., Xiao, M., Lin, Q. & Fan, S. Synthetic space with arbitrary dimensions in a few rings undergoing dynamic modulation. *Phys. Rev. B* **97**, 104105 (2018).
50. Loring, T. A. & Hastings, M. B. Disordered topological insulators via C*-algebras. *Europhys. Lett.* **92**, 67004 (2010).
51. Szameit, A. et al. Discrete optics in femtosecond-laser-written photonic structures. *J. Phys. At. Mol. Opt. Phys.* **43**, 163001 (2010).

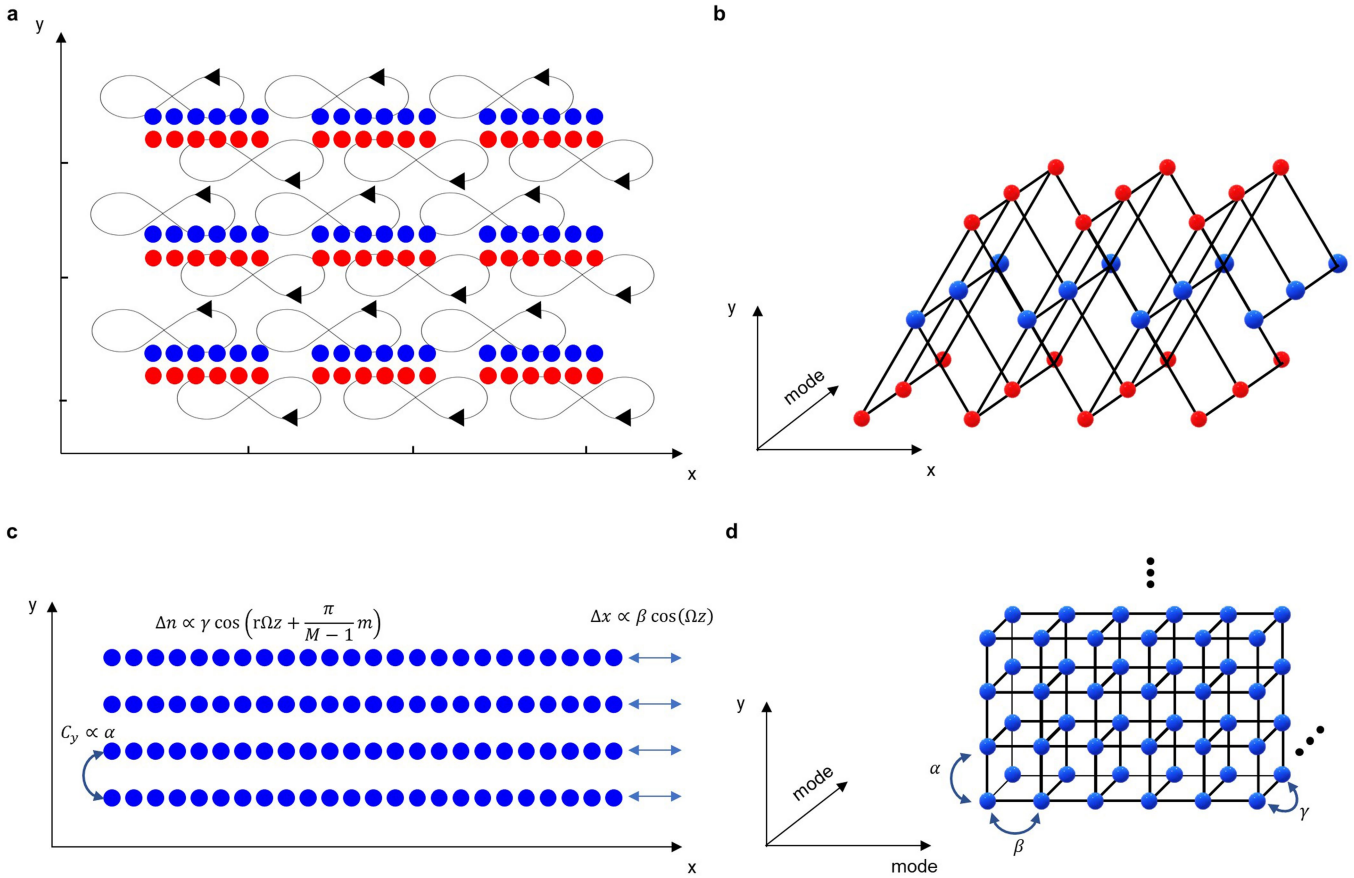

Extended Data Fig. 1 | Increasing the dimensionality of a two-dimensional lattice of waveguides. a, One-dimensional columns arranged in a two-dimensional lattice. The columns oscillate along the black paths in the direction indicated by the triangles. Red and blue colours indicate different columns in the same unit cell. **b**, Representation of **a** in synthetic dimensions. **c**, Lattice with two oscillation frequencies, oscillating in the x direction according to Δx and with index of refraction changing periodically according to Δn. **d**, Representation of **c** in synthetic dimensions.

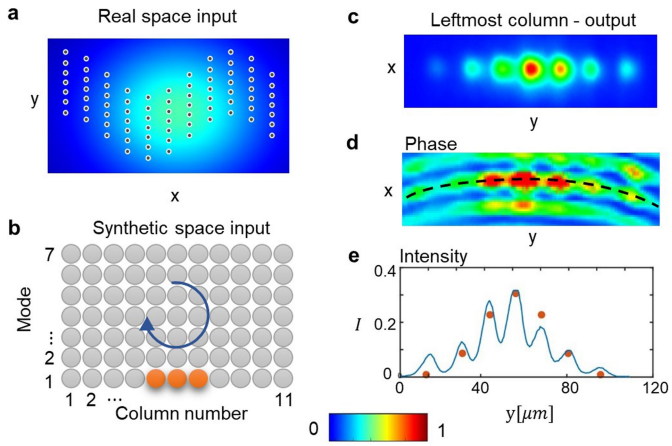

Extended Data Fig. 2 | Light occupancy in the leftmost column when a Gaussian beam is launched from the middle of the lattice. **a**, **b**, Illustrated intensity (colour bar; peak intensity is set to 1) of the initial Gaussian beam launched in real space (**a**) and synthetic space (**b**). **c**, Measured output intensity of the leftmost column for the input shown in **a** and **b**. **d**, Measured interference of the lattice output at the leftmost column with the input beam, showing that all of the seven peaks are in phase (the dashed line represents equal phase), indicating that the light at the leftmost column occupies the lowest spatial mode of the column. **e**, Measured normalized intensity cross-section (blue line) at the leftmost column of the lattice output, compared with the theoretically calculated (tight-binding) intensity profile of the first mode of the column (orange circles). The sum of peak intensities is normalized to 1.

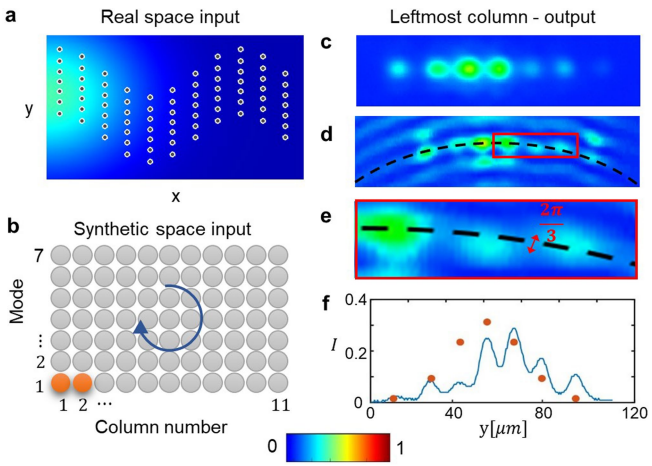

Extended Data Fig. 3 | Light occupancy in the leftmost column when a Gaussian beam is launched from the left side of the lattice. **a**, **b**, Illustrated intensity pattern (colour bar) of the initial Gaussian beam launched in real space (**a**) and in synthetic space (**b**). **c**, Measured intensity distribution at the leftmost column. **d**, Measured interference pattern at the lattice output at the leftmost column, showing that, unlike in Extended Data Fig. 2d, the seven intensity peaks are not in phase and therefore occupy higher modes of the array. **e**, Zoom-in on the red rectangle in **d**, showing that the light peaks are not aligned on the equal-phase line (dashed line). **f**, Cross-section (blue line) of the intensity pattern at the leftmost column of the lattice output, compared with the calculated intensity profile of the first mode (orange circles) where the sum of peak intensities is normalized to 1. The mismatch shows that the light is occupying modes higher than the first mode.

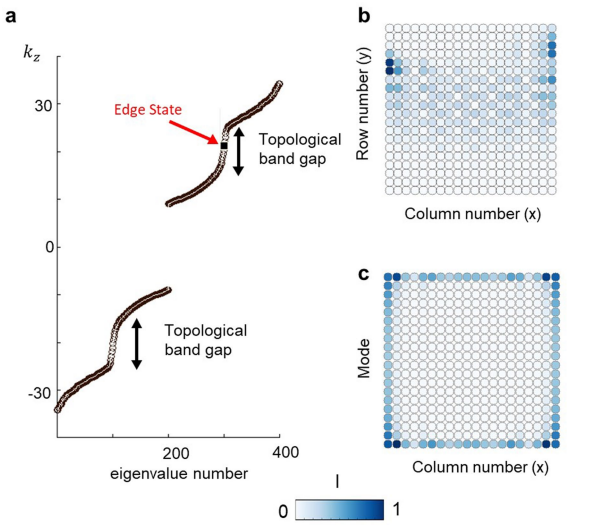

Extended Data Fig. 4 | Floquet spectrum of equation (1). a, Eigenvalues obtained numerically for a 20 × 20 site, displaying two topological gaps. **b**, Real-space amplitude distribution of an eigenstate residing in the gap (edge state marked in **a**). **c**, The same eigenstate as in **b** as it appears in synthetic space (unitary transformation of **b**), showing clearly that the marked state is an edge state. The parameters used are $R = 5\,\mu m$, $\Omega = 69.1448\ m^{-1}$, coupling in y $cy = 10.9431\ m^{-1}$ and $k0 = 1.9 \times 10^7\ m^{-1}$.

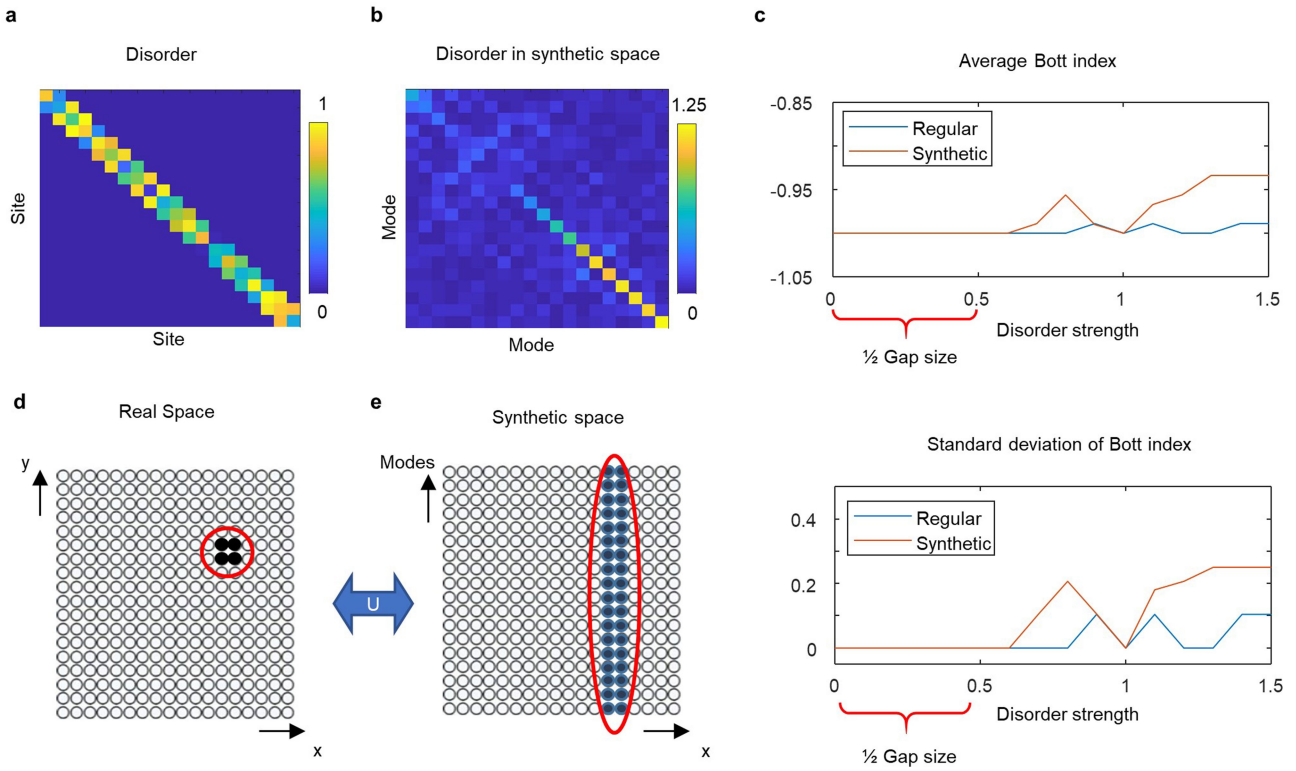

Extended Data Fig. 5 | Disorder in synthetic space. a, Typical disorder introduced to the Hamiltonian of a one-dimensional lattice. The Hamiltonian is in real-space matrix representation (the colour bar corresponds to the real part of the value of the matrix element). **b**, The disorder shown in **a** after transformation to synthetic space. **c**, Standard deviation and mean value of the Bott index averaged over 10 random disorder realizations for the regular topological insulator (blue line) and for the topological insulator in synthetic dimensions (red line). The red bracket indicates half of the bandgap. **d**, **e**, A disorder (black sites) that is confined spatially in real space is not confined in synthetic space (blue sites).

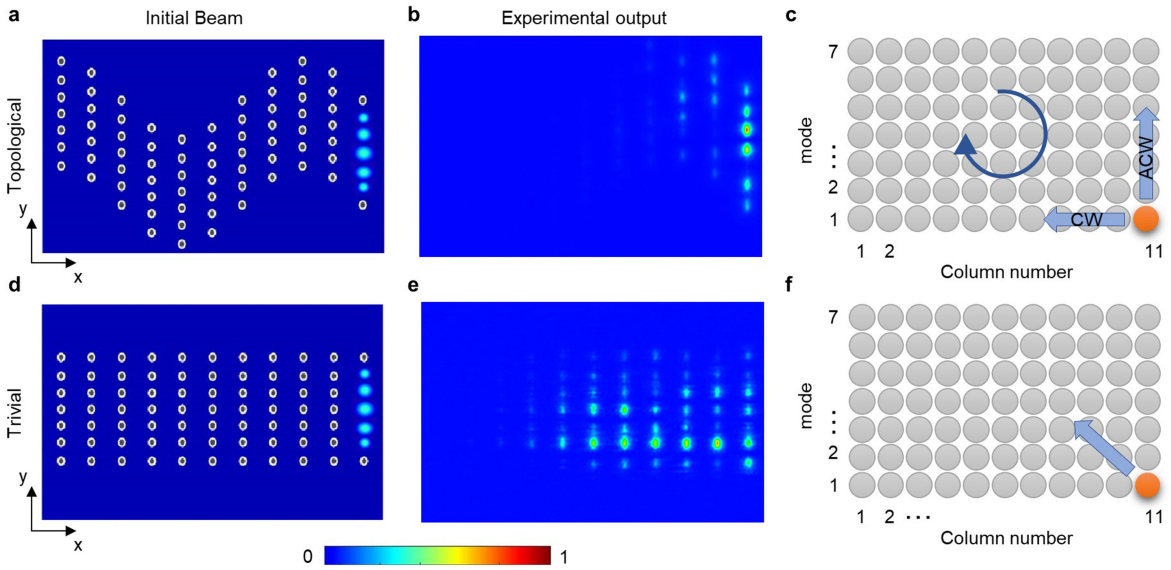

Extended Data Fig. 6 | Exciting the anticlockwise edge state. a, Initial excitation of the first mode in the rightmost column of the topological lattice. **b**, Output intensity (colour bar) corresponding to **a**. **c**, Direction of propagation of the light in synthetic space. **d**–**f**, The same as **a**–**c**, but for the trivial lattice. CW, clockwise; ACW, anticlockwise.

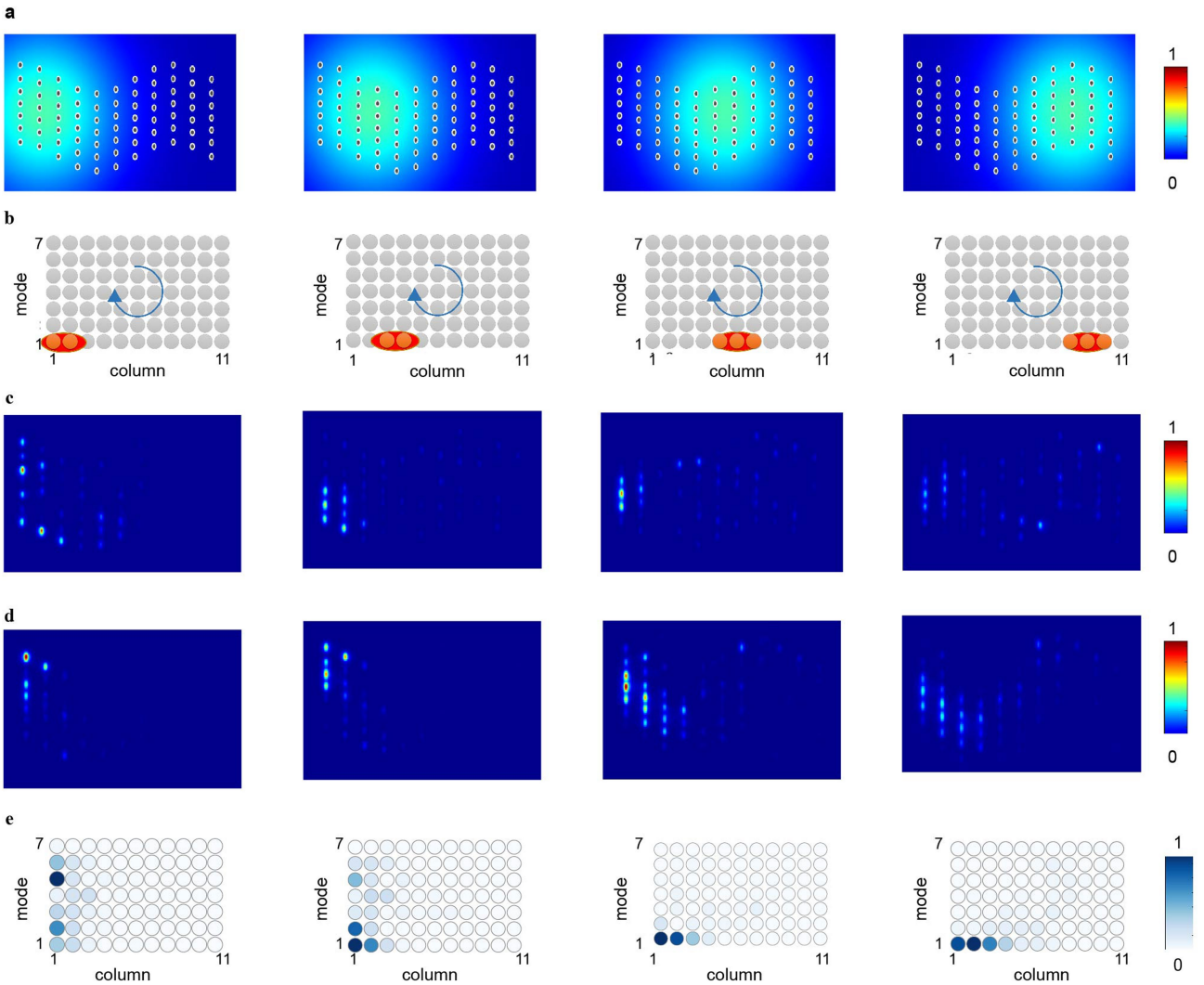

Extended Data Fig. 7 | Experimental results for a sample fabricated with different parameters. Illustration of an incident narrow Gaussian beam directed towards the input facet of a synthetic-space topological lattice fabricated with parameters different from those used in the experiments presented in the main text (here, $\phi = \pi/4$, $\Omega = 91\ \mathrm{m}^{-1}$ and $R = 17.5\ \mu\mathrm{m}$). **a**, **b**, Input beam launched at different locations in real space (**a**) and synthetic space (**b**). **c**, **d**, Experimentally imaged (**c**) and simulated (**d**) beam intensity at the output facet of the lattice. **e**, Synthetic-space description corresponding to the evolution of the wavepacket as it propagates in the lattice.

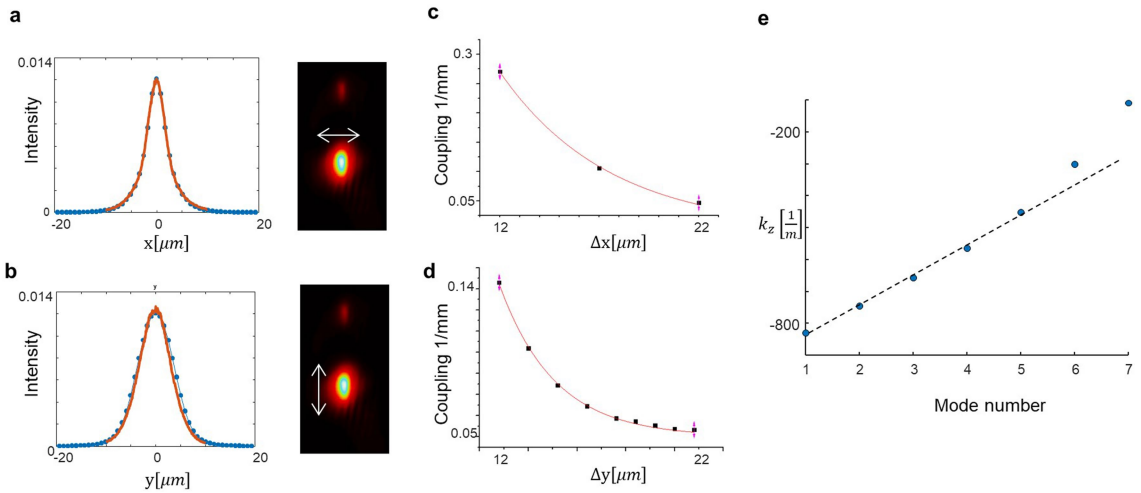

Extended Data Fig. 8 | Stages in the preparation of the experimental model. a, Horizontal cross-section of the intensity of a propagating mode of a single waveguide (orange line) and the cross-section of the mode in the simulations (blue line). The image on the right is the intensity distribution of the mode in the direction of the cross-section. **b**, Same as **a**, but for the vertical cross-section of the propagating mode of a single waveguide. **c**, Coupling versus distance in the horizontal direction. **d**, Coupling versus distance in the vertical direction. **e**, Mode propagation constants of the J_x lattice based on measured experimental parameters (blue circles). The dashed line is a guide for the eye.